Electric Power Systems Research 193 (2021) 106974

Contents lists available at ScienceDirect

Electric Power Systems Research

journal homepage: www.elsevier.com/locate/epsr

A decentralized approach for frequency and voltage regulation in islanded PV-Storage microgrids

A. Rosini [a], D. Mestriner [a], A. Labella [a], A. Bonfiglio [a,*], R. Procopio [a]

[a] University of Genoa, Department of Electrical, Electronic, Telecommunications Engineering and Naval Architecture, Via Opera Pia 11a– I-16145, Genoa, Italy

ARTICLE INFO

Keywords:
Photovoltaic integration
Primary frequency control
Voltage regulation
Renewable Energy Sources
Model Predictive Control

ABSTRACT

This paper proposes a novel decentralized and communication-less control strategy for frequency and voltage regulation in Photovoltaic (PV)-Storage islanded Microgrids (MGs). The developed approach aims at achieving a suitable management of the different operational assets of the PV-Storage islanded MGs providing seamless transitions among them and guaranteeing a continuous and effective power supply to the loads. Local inverter controllers are designed exploiting the capabilities of the Model Predictive Control; the resulting control architecture is a composition of local Distributed Generating (DG) unit controller relies only on measurements available on the DG unit site that allows nullifying both frequency and voltage errors providing a suitable repartition of the power request. This way, the proposed approach can combine the advantages of the classic droop and master/slave controllers as it needs neither communication among devices nor a secondary centralized control loop. Moreover, it is able to account for the Storage characteristics imposing a power curtailment of the PV units whenever either the power absorption or the State of Charge limit is reached.

1. Introduction

One of the most important challenges of the energy sector for the current century is the massive deployment of Renewable Energy Sources (RES) in order to aim at a sustainable and environmentally friendly energy supply.

The transition to such scenario requires an evolution of the current way the electricity system is managed since the increasing of stochastic power generation will demand a consequent improvement of the system flexibility [1,2]. This is witnessed by numerous initiatives and calls for projects at international and European level aiming at proposing flexibilization of power generation, transmission [3], distribution and consumption [4-6].

In this context, the most promising concept to integrate RES source into the energy mix in a flexible and efficient way is represented by the so called Microgirds (MGs). A MG is defined as an integrated energy system consisting of distributed energy resources and multiple electrical loads operating as a single, grid either in parallel to, or islanded from the existing distribution power grid [7].

Among the various MGs set-ups, the one that is collecting some relevant interest from producers, customers and researchers is the so called autonomous Photovoltaic (PV) -Storage configuration [8]. The reason of this interest lays in the large amount of PV installations all over the world and the idea that efficiently shifting the production capability of PV plants will significantly improve their exploitability. Moreover, a PV-Storage MG can also be self-sustainable if properly designed [9] providing an important contribution to the electrification of rural areas and to the flexibility and resiliency of existing electric networks in case of possible islanding of the sub-system.

Beside the simplicity of the idea to integrate PV and Storage devices, many are the problems to be faced to efficiently do it, especially if an islanded PV-Storage MG is considered [10]. In this latter case, the system needs to be capable to satisfy the load demand, providing frequency and voltage regulation, but also to suitably manage the Storage State Of Charge (SOC) in order to guarantee the continuity of supply to the MG loads. Nevertheless, making a PV-Storage system an islanded MG will allow the possibility of intentionally island the PV generation in case the distribution system should face unreliable operational conditions due to variations of the stochastic generation. For this reason, the focus of the present article is the definition of an innovative control logic for the correct operation of an islanded PV-Storage MG.

In general, primary MGs frequency and voltage control strategies can be divided into two main categories depending on the need of an Information&Communications Technology (ICT) infrastructure or not

* Corresponding author.
E-mail address: a.bonfiglio@unige.it (A. Bonfiglio).

https://doi.org/10.1016/j.epsr.2020.106974
Received 20 April 2020; Received in revised form 13 October 2020; Accepted 19 November 2020
Available online 22 January 2021

[11]. ICT based MG control techniques include the so called master/-slave control [12,13] and distributed control [14]. On the other side, among the communication-less primary regulation approaches it is worth citing the droop control [15] and its numerous variants [16]. The main problems of ICT based primary controllers are related to the need for high-bandwidth communication channels, which can be impractical, vulnerable and expensive in MGs with long connection distances among generating units. On the other hand, the droop approach for primary regulation implies two main drawbacks: *i*) frequency and voltage deviations from their rated values, resulting in the need of secondary regulation, and *ii*) the inability to satisfy multiple control objectives [11]. Moreover, from an applicative point of view, droop approaches suffer sensitivity issues on frequency variation imposing to provide an inertial behavior to frequency response. This implies the installation of a diesel generators [17] or the implementation of a "Virtual Synchronous Generator" control in the Storage power converter [18] with a consequent increasing of the topological or technical complexity of the system.

In this frame, the control of islanded PV-Storage configurations was deeply investigated in literature. Previous works focused their attention on solutions where the PV unit and the battery share the same converter [19,20]. Such a configuration is quite limiting since it cannot be applied for the retrofit of existing PV plants or for configurations where the PV and the Storage are not installed close to each other. Beside this solution, recent works tried to solve this issue with smart control approaches using the system frequency as a communication signal but without the necessity to install additional devices. In particular, [21] shows a PV-Storage management where each generation unit is equipped with a dedicated local primary controller and the frequency produced by each inverter is used to give and receive information about the operational status of the system. The main drawback of [21] is that it needs a secondary controller to restore the MG frequency at its rated value; moreover, it does not take into account the bounds on the system frequency and on the rating of the inverter, limitation that could strongly affect the proper operation of the system. Recently [22-24], some researchers have tried to adapt the Model Predictive Control (MPC) approach to the primary control of islanded MGs. It must be underlined that [22-24] is one of the very few cases where MPC is proposed for component control rather than for secondary and tertiary control [25,26]. The authors of [27] proposed a MPC with improved droop controller for parallel operated power inverters in islanded MG; compared with classical controller, this method has a more compact structure meanwhile requiring less tuning effort. However, the method is still based on the droop techniques, leading to the well-known problem in terms of offset of the steady-state frequency. Another important work has been presented in [24], where the authors introduced a primary regulator for the energy storage inverters able to improve the response time, the power and voltage ripples and the frequency spectrum with respect to the traditional PID technique; however, their application is limited to the energy storages and does not present any possible solution for the control of PV inverters as well as any common strategies among the devices. In [22] and [23], the authors proposed to replace traditional PID based ones for the control of inverters fed by renewable power generation. However, in [22] and [23] the MPC controller is only used to merely substitute the classical PID ones but is inserted in a traditional (or adapted [23]) droop-based scheme. Consequently, the method presented in [22] does not nullify the system frequency error, while [23] needs a not-trivial adjustment of the control parameters related to the adapted droop control; in particular the derivative term included in the droop-control laws can cause unexpected oscillations. Moreover, no hint is provided on the management of different operational assets of the PV-Storage MG (e.g. SOC saturation, Storage power limitations, PV production curtailment, etc.).

So, the aim of the present article is to start from the idea developed in [22] and [23] to design local inverter controllers that better exploit the features of the MPC (i.e. predicting the future behavior of the system and inserting constraints on the variables) providing a plug-and-play control architecture for the islanded PV-Storage system. Such architecture shall meet both the primary and secondary controller goals (sharing the load request among the sources and zeroing the frequency errors) without the need of an ICT infrastructure (i.e. based only on local measurements). The main innovative contributions provided by the proposed decentralized MPC architecture are:

- combining the advantages of the droop and master/slave controllers (no communication needed and frequency and voltage restoration);
- defining suitable converter controllers capable to manage the storage SOC and power limitations and PV converters curtailment;
- guarantee an automatic and seamless transition among the different MG operating assets without communication;
- Combining in one (local) controller for each device the jobs of traditional primary and secondary frequency regulation.

2. General overview and structure of the proposed control architecture

The considered MG configuration consists of a Storage unit and N_{PV} PV systems, each interfaced with the AC MG distribution system via power electronics converter, as depicted in Fig. 1, where for the *i th* PV C_{PVi} is the DC-link capacitance, $R_{f,PVi}$, $L_{f,PVi}$ and $C_{f,PVi}$ are the harmonic filter resistance, inductance and capacitance respectively, $V_{inv,PVi}$ is the voltage phasor at the output of the PV inverter and $V_{ac,PVi}$ is the voltage phasor at the output of the PV harmonic filter. For the Storage unit, R_{ST}, L_{ST} and C_{ST} are the resistance, inductance and capacitance of the DC-link respectively, $R_{f,ST}$, $L_{f,ST}$ and $C_{f,ST}$ are the harmonic filter resistance, inductance and capacitance respectively, $V_{inv,ST}$ is the voltage phasor at the output of the Storage inverter and $V_{ac,ST}$ is the voltage phasor at the output of the Storage harmonic filter. The assumption of considering many PV units is related to the fact that large PV plants are organized in sub-fields each provided with a dedicated converter in order to suitably manage a fixed number of PV strings [28] while typically even very big storage systems are connected to the MG with only one inverter. In the proposed architecture, each PV and Storage converter is equipped with a local controller (please note that the structure of the Storage controller is different from the PV ones, as will be clarified later on).

As specified in the introduction, the control objectives of such architecture are the following:

1) restoring the system frequency and voltage after a contingency without any communication systems among the local controllers (i.e. the proposed structure combines the action of the classic primary and secondary frequency and voltage regulators with no need of communication links);
2) guaranteeing the possibility of new PV units plug-and-play;
3) accounting for the storage technical limits in terms of SOC and maximum absorption/injection power. This implies that when the storage power and SOC are within the limits, the PV units must work at their MPP; while their power production must be curtailed when one of such limits is violated.

So three main MG configurations can be defined for the unit controllers, namely the Normal Operation (NO), Storage Power Priority (PP) and Storage SOC Priority (SP) [29]. The MG NO is when the load request and the PV Maximum Power Point production are not causing any violation of the Storage power and SOC limits. In this configuration, the PV units local controllers make them work at their MPP, while the Storage controller makes it act as an independent voltage source in order to achieve the active and reactive power balance. The PP operation mode corresponds to a condition when the Storage should absorb a power greater than its rating and thus it is necessary to limit its power at the maximum absorption threshold while the PV controllers must curtail their production to satisfy the power balance. Finally, the SP mode is

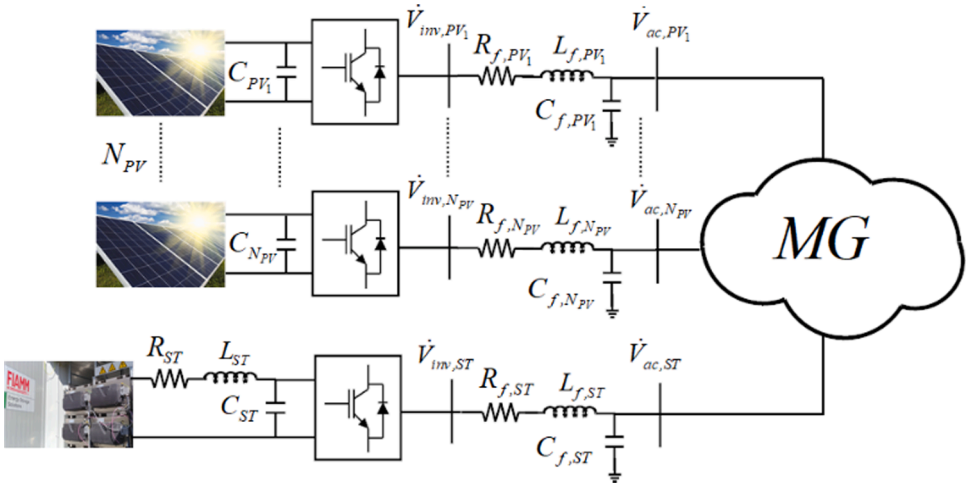

Fig. 1. General PV-Storage MG layout.

activated when the Storage reaches its maximum SOC; in this case the Storage controller needs to nullify the Storage power absorption and, once again, the PVs must curtail their production to balance the load demand. As a result, the Storage controller accounts for three different operational modes, while the PV controller accounts for only two operational modes since the PV behavior in PP and SP modes is exactly the same (for this reason in the following this will be labelled as CURT for the PV MPC controllers). All the possible combinations are summarized in Table 1. Fig. 2 shows a high level diagram for the operating mode for the Storage (ST) and PV converters. Green bubbles represent the NO modes, while the red bubbles are the curtailed mode for the PV and the PP and SP modes for the storage. Green lines are the transitions to NO modes, while red lines are the transitions to the PP and SP modes. The transitions triggering logics are described in detail in Section 3.3.

For the sake of completeness two other scenarios can happen when the load request is greater than the overall PV MPP production and *i*) the Storage is providing its maximum power injection and *ii*) the Storage is totally discharged i.e. the SOC is at its lower limit value. Nevertheless, these two cases can only be managed reducing the load request and (for example via some Demand Response strategies); for this reason, they are disregarded in the present paper.

3. MPC controller design

As well known, an MPC controller acts to regulate the state $\mathbf{x}$ of the system to a reference value $\mathbf{x}_{ref}$ by solving a constrained Quadratic-Programming problem where the objective function is a quadratic form in the state error $\mathbf{e}_k = \mathbf{x}_{ref,k} - \mathbf{x}_k$ defined as follows:

$$\min_{\boldsymbol{u}_{k+i}} \quad \boldsymbol{e}_{k+N}^T Q \boldsymbol{e}_{k+N} + \sum_{i=0}^{N-1} \left\{ \boldsymbol{e}_{k+i|k}^T Q \boldsymbol{e}_{k+i|k} + \left(\boldsymbol{u} - \boldsymbol{u}_{ref}\right)_{k+i}^T R \left(\boldsymbol{u} - \boldsymbol{u}_{ref}\right)_{k+i} \right\} \tag{1}$$

where $\boldsymbol{u}_k$ is the optimal input vector (i.e. the control law to be ordered to the system at time step k), $\boldsymbol{u}_{ref,k}$ its corresponding reference value, $\boldsymbol{e}_{k+i|k}$ is the state error predicted for step $k+i$ at step k.

Q and R are symmetric and positive semi-definite weighting matrices. MPC controllers can also account for linear (equality and inequality) constraints in the system states and inputs. For the interested reader more details on the MPC can be found in [30].

Table. 1
System operation modes and converter control modes.

	Storage converter	PV converter
NO mode	NO	NO
PP mode	PP	CURT
SP mode	SP	CURT

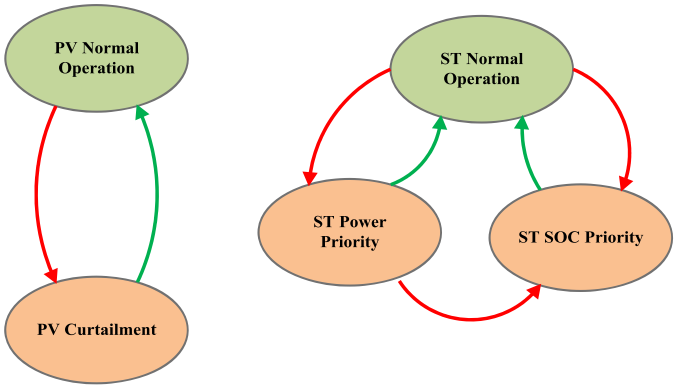

Fig. 2. System operation modes and Converter control modes diagram. Green lines are the transitions to the NO modes from the other operating modes, while the red lines are the transitions to the PP and SP modes.

To reach the goals defined in the previous section, the following steps are necessary:

1) Definition of the objective function and of the constraints for the PV controller (Section 3.1) and for the storage controller (Section 3.2);
2) Definition of the weights Q and R in the objective function of the two controllers in the different system operation modes (SubSection 3.1.1 and 3.1.2 for the PV converter and SubSection 3.2.1, 3.2.2 and 3.2.3 for the storage converter);
3) Definition of the logics for the automatic transition among the system operation modes.

As far as the first point of the above checklist is concerned, it is necessary to define a suitable dynamic model of PV and storage that, once discretized, will represent part of the MPC optimization problem constraints. Such model, from now on "auxiliary model", must be sufficiently simple to reduce the computational complexity of the algorithm but sufficiently accurate to properly describe the real system dynamics. In the proposed approach, such model relies on the following assumptions:

- the MG AC section is supposed to be at steady-state;
- inverters are supposed to work in their linear range;
- inverters efficiency is assumed to be unitary;
- higher order harmonics are neglected;

- shunt and resistive component of harmonic filters are neglected.

Such modeling has been extensively validated against experimental measurements in [31]. However, for the sake of clarity, it is worth pointing out that these assumptions are only made for the controllers' design. The simulations presented in Section IV have been carried out using the controllers designed according to the auxiliary model, but the power system is described selecting for each device the most complete model available in the Simulink/Simscape® library. Therefore, the presence of dynamics or phenomena that have been neglected in the regulator design allow to test the control system robustness.

3.1. PV inverters controller design

Considering one of the N_{PV} units connected to the MG as in Fig. 1, the line-to-ground RMS inverter output voltage is:

$$\dot{V}_{inv,PV}(t) = \frac{m_{a,PV}(t)V_{dc,PV}(t)}{2\sqrt{2}} e^{j\theta_{PV}(t)} \tag{2}$$

where $m_{a,PV}$ is the inverter modulation index, $V_{dc,PV}$ is the DC-link voltage and $\theta_{PV}(t)$ is given by:

$$\theta_{PV}(t) = \int_0^t \omega_{PV}(\tau)d\tau + \theta_{PV0} \tag{3}$$

where ω_{PV} is the angular frequency of the PV inverter modulation signals and θ_{PV0} is the PV system initial phase. The PV voltage at the harmonic-filter output can be written as:

$$\dot{V}_{ac,PV}(t) = V_{ac,PV}(t)e^{j\theta_{f,PV}(t)} \tag{4}$$

where $V_{ac,PV}$ is the line-to-ground voltage at the harmonic-filter output and $\theta_{f,PV}(t)$ is given by:

$$\theta_{f,PV}(t) = \int_0^t \omega_{f,PV}(\tau)d\tau + \varphi_{f,PV}(t) \tag{5}$$

$\omega_{f,PV}$ being the AC-bus angular frequency measured via PLL and $\varphi_{f,PV}(t)$ the phase angle of $V_{ac,PV}$. For the sake of readability, from now on the explicit time dependence will be omitted. Under the active sign convention, the active power flow injected by the PV unit into the MG is given by:

$$P_{ac,PV} = 3\frac{m_{a,PV}V_{dc,PV}V_{ac,PV}}{2\sqrt{2}x_{f,PV}}\sin\left(\theta_{PV} - \theta_{f,PV}\right) \tag{6}$$

where $x_{f,PV}$ is the longitudinal reactance of the harmonic-filter calculated at the MG rated angular frequency. Substituting (3) and (5) in (6) one can easily obtain:

$$P_{ac,PV} = \frac{3m_{a,PV}V_{dc,PV}V_{ac,pV}}{2\sqrt{2}x_{f,PV}}\sin\left(\theta_{PV0} - \varphi_{f,PV} + \int_0^t \left(\omega_{PV} - \omega_{f,PV}\right)d\tau\right) \tag{7}$$

Let us now define:

$$\sigma_{PV} = \theta_{PV0} - \varphi_{f,PV} \tag{8}$$

and

$$\delta_{PV} = \int_0^t \left(\omega_{PV}(\tau) - \omega_{f,PV}(\tau)\right)d\tau, \tag{9}$$

inserting (8) and (9) into (7) one obtains:

$$P_{ac,PV} = 3\frac{m_{a,PV}V_{dc,PV}V_{ac,PV}}{2\sqrt{2}x_{f,PV}}\sin(\sigma_{PV} + \delta_{PV}). \tag{10}$$

Moreover, the DC-link voltage dynamic is:

$$P_{dc,PV} - P_{ac,PV} = V_{dc,PV}C_{PV}\frac{dV_{dc,PV}}{dt} \tag{11}$$

C_{PV} being the DC-link capacitor and $P_{dc,PV}$ the power coming from the PV unit that depends on the DC voltage $V_{dc,PV}$, the solar irradiance α and the PV cells temperature T, as follows (see [32] for its explicit expression):

$$P_{dc,PV} = I_{dc,PV}\left(V_{dc,PV}, \alpha, T\right)V_{dc,PV}. \tag{12}$$

Substituting (10) and (12) in (11), one has:

$$\begin{cases} \dfrac{dV_{dc,PV}}{dt} = \dfrac{1}{C_{PV}}\left[I_{dc,PV}\left(V_{dc,PV}, \alpha, T\right) - \dfrac{3m_{a,PV}V_{ac,PV}}{2\sqrt{2}x_{f,PV}}\sin(\sigma_{PV} + \delta_{PV})\right] \\ \dfrac{d\delta_{PV}}{dt} = \omega_{PV} - \omega_{f,PV} \end{cases}. \tag{13}$$

System (13) is a non-linear continuous-time system in the form:

$$\dot{\boldsymbol{x}}_{PV} = f(\boldsymbol{x}_{PV}, \boldsymbol{u}_{PV}, \boldsymbol{g}_{PV}) \tag{14}$$

where $\boldsymbol{u_{PV}} = [m_{a,PV}\ \omega_{PV}]^T$ is the input vector, $\boldsymbol{x_{PV}} = [V_{dc,PV}\ \delta_{PV}]^T$ is the state vector and $\boldsymbol{g_{PV}} = [V_{ac,PV}\ \sigma_{PV}\ \alpha\ T\ \omega_{f,PV}]^T$ is a vector that collects measurements and estimated variables. In particular, $V_{ac,PV}$, α, T and $\omega_{f,PV}$ can be easily measured, while σ_{PV} can be estimated measuring the PV AC side active power and inverting (10) as follows:

$$\sigma_{PV} = \sin^{-1}\left(\frac{2\sqrt{2}P_{ac,PV}x_{f,PV}}{3m_{a,PV}V_{dc,PV}V_{ac,PV}}\right) - \int_0^t \left(\omega_{PV}(\tau) - \omega_{f,PV}(\tau)\right)d\tau. \tag{15}$$

The mathematical model used for prediction by the MPC controller can be put in the classical linear representation as in [30] according to the following steps:

- Linearizing (13) around the value of the state assumed at each time instant in which the MPC algorithm has to be run
- Discretizing the resulting linear system supposing to sample the original continuous system with sampling time T_s
- Transforming measurements collected in vector $\boldsymbol{g_{PV}}$ into states with no dynamics. This is necessary because the MPC needs a dynamic model over the whole prediction horizon but of course the time evolution of measurements is unknown during the prediction.
- Transforming the modulation index $m_{a,PV}$ into a state considering its derivative J_{PV} as an input, to be regulated to zero. This because it is important that the modulation index is constant at steady state no matter the value it assumes in its operational range.

Details on these steps are provided in Appendix.

The resulting PV unit model is:

$$\tilde{\boldsymbol{x}}_{PV,k+1} = A_{PV}\tilde{\boldsymbol{x}}_{PV,k} + B_{PV}\tilde{\boldsymbol{u}}_{PV,k} + h_{PV} \tag{16}$$

where:

$$\tilde{\boldsymbol{x}}_{PV,k} = \begin{bmatrix} \boldsymbol{x}_{PV,k} & \boldsymbol{g}_{PV,k} & m_{a,PV,k} \end{bmatrix}^T \tag{17}$$

$$\tilde{\boldsymbol{u}}_{PV,k} = \begin{bmatrix} \omega_{PV,k} & J_{PV,k} \end{bmatrix}^T \tag{18}$$

while

$$\tilde{\boldsymbol{u}}_{ref,PV,k} = \begin{bmatrix} 2\pi f_r & 0 \end{bmatrix}^T \tag{19}$$

f_r being the rated frequency. Expressions for the matrices involved in the above equations can be found in Appendix.

Additional constraints included in the PV MPC controller are listed in the following. The PV unit frequency does not have to exceed the minimum limit f_{min} and the maximum limit f_{max}, so:

$$2\pi f_{\min} \le \omega_{PV,k} \le 2\pi f_{\max}. \tag{20}$$

The modulation index is constrained in order to guarantee the inverter working in its operational range [33]:

$$m_{a,\min} \leq m_{a,PV,k} \leq m_{a,\max}. \tag{21}$$

Furthermore, according to the local DSO requirements, regulation of the PV unit reactive power exchange has to be performed. The reactive power Q_{PV} injected by the PV unit, calculated as:

$$Q_{PV} = 3\left[\frac{m_{a,PV}^2 V_{dc,PV}^2}{8x_{f,PV}} - \frac{m_{a,PV} V_{dc,PV} V_{ac,PV}}{2\sqrt{2}x_{f,PV}}\cos(\sigma_{PV} + \delta_{PV})\right] \tag{22}$$

Reactive power regulation can be done linearizing and discretizing (22) and imposing the following constraint:

$$-\varepsilon_Q + Q_{PV,ref} \leq Q_{PV,k} \leq Q_{PV,ref} + \varepsilon_Q \tag{23}$$

$Q_{PV,ref}$ being the reactive power reference and ε_Q half the amplitude of the admissible reactive power error. Finally, the inverter capability curve can be linearized and discretized in order to impose:

$$\sqrt{P_{ac,PV,k}^2 + Q_{PV,k}^2} \leq A_{PV} \tag{24}$$

A_{PV} being the inverter rating.

Consequently, at each time step kT_s the MPC controller for the PV unit solves the following optimization problem:

$$\begin{aligned} \min_{\boldsymbol{u}_{k+i}} \quad & \boldsymbol{e}_{PV,k+N}^T \boldsymbol{Q} \boldsymbol{e}_{PV,k+N} + \sum_{i=0}^{N-1} \Big\{ \boldsymbol{e}_{PV,k+i|k}^T \boldsymbol{Q} \boldsymbol{e}_{PV,k+i|k} \\ & + \left(\widetilde{\boldsymbol{u}}_{PV} - \widetilde{\boldsymbol{u}}_{ref,PV}\right)_{k+i}^T R \left(\widetilde{\boldsymbol{u}}_{PV} - \widetilde{\boldsymbol{u}}_{ref,PV}\right)_{k+i} \Big\} \end{aligned} \tag{25}$$

where $\boldsymbol{e}_{PV,k} = \widetilde{\boldsymbol{x}}_{ref,PV,k} - \widetilde{\boldsymbol{x}}_{PV,k}$ and

$$\begin{aligned} \widetilde{\boldsymbol{x}}_{ref,PV,k} = \Big[& V_{dc,ref,PV,k} \quad \delta_{ref,PV,k} \quad V_{ac,ref,PV,k} \quad \sigma_{ref,PV,k} \quad \alpha_{ref,k} \\ & T_{ref,k} \quad \omega_{f,ref,PV,k} \quad m_{a,ref,PV,k} \Big]^{\mathrm{T}} \end{aligned} \tag{26}$$

subject to: system predicted dynamics (16), bound on frequency (20) and on modulation index (21), reactive power regulation (23) and capability curve (24).

Numerical values of the reference signals in (26) and of the weighting matrices Q and R depend on the operational mode of the controller (which will be clarified in the next section). The resulting configuration of the PV MPC controller is depicted in Fig. 3 where one can notice that only PV unit local measurements are necessary.

3.1.1. PV controller–normal operation

In NO operation mode, the PV unit has to produce its maximum power and contribute to the frequency and voltage regulation with the injection/absorption of reactive power. Consequently, the goals of PV MPC controller in NO are to regulate the PV DC-link voltage $V_{dc,PV}$ to its MPP value $V_{mpp,PV}$, restoring ω_{PV} to its rated value and bringing J_{PV} to zero. $V_{mpp,PV}$ is obtained using the open voltage method (see [34]) in order to avoid iterative procedures. Under these considerations the definition of the weighting matrices for the PV MPC controller in NO are the following:

$$\begin{cases} Q = Q_{PV-NO} = diag\left(q_{V_{dc}}^{PV}, 0_{1\times 7}\right) \\ R = R_{PV-NO} = diag\left(r_{\omega}^{PV}, r_{J}^{PV}\right) \end{cases} \tag{27}$$

As a consequence the only meaningful value in (26) is the one of the DC voltage, i.e. $V_{dc,ref,PV,k} = V_{mpp,PV}$, while all that other values are useless because the corresponding weights in (27) are zero.

3.1.2. PV controller – curtailment control mode

In CURT operation modes the PV unit controller needs to stop following its DC $V_{mpp,PV}$ providing a curtailment of the active power production in order to guarantee the MG power balance. This implies that, when the CURT mode is triggered, also the weight corresponding to the DC voltage becomes zero, leading to the following weighting matrices:

$$\begin{cases} Q = Q_{PV-CURT} = diag(0_{1\times 8}) \\ R = R_{PV-CURT} = diag\left(r_{\omega}^{PV}, r_{J}^{PV}\right) \end{cases} \tag{28}$$

3.2. Storage inverter MPC controller design

The mathematical model used for the design procedure of the Storage MPC controller is the following:

$$\begin{cases} \dfrac{dV_{dc,ST}}{dt} = \dfrac{1}{C_{ST}}\left[I_{dc,ST} - \dfrac{3m_{a,ST}V_{ac,ST}}{2\sqrt{2}x_{f,ST}}\sin(\sigma_{ST} + \delta_{ST})\right] \\ \dfrac{d\delta_{ST}}{dt} = \omega_{ST} - \omega_{f,ST} \\ \dfrac{dI_{dc,ST}}{dt} = \dfrac{E(SOC) - R_{ST}I_{dc,ST} - V_{dc,ST}}{L_{ST}} \\ \dfrac{dSOC}{dt} = -\dfrac{I_{dc,ST}}{NCC} \end{cases} \tag{29}$$

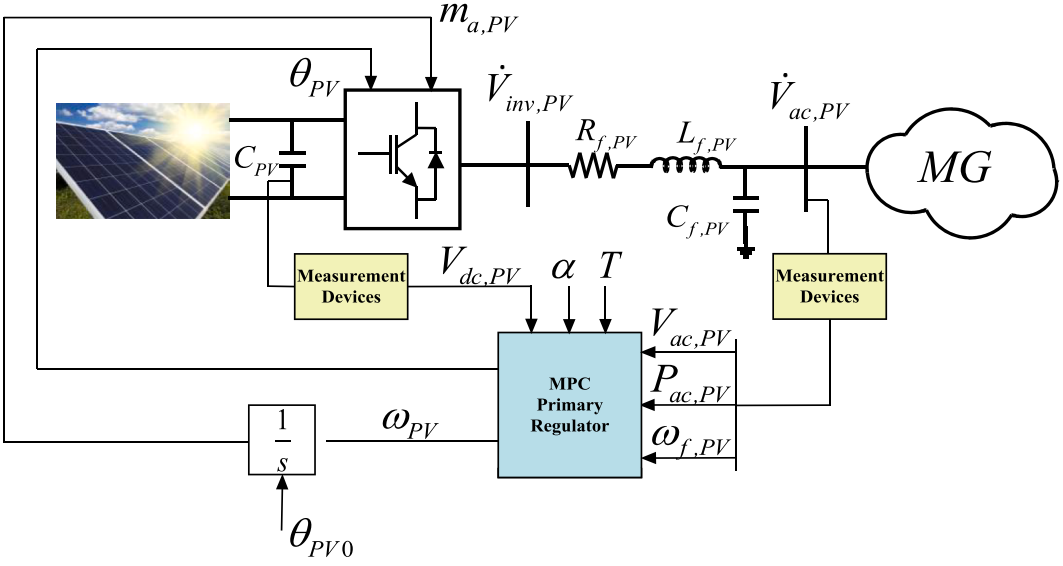

Fig. 3. PV control scheme.

where $I_{dc,ST}$ is the Storage DC-current, E is the Storage internal voltage depending on its SOC, R_{ST} and L_{ST} are the Storage internal resistance and inductance respectively and NCC is the Nominal Current Capacity. The first two equations of (29) have the same meaning as for the PV MPC controller, the third is the DC R-L circuit dynamics (see Fig. 1) and the fourth is the relationship between the Storage DC current and the SOC (see [35] for details). Following the same procedure used for the definition of the PV MPC controller, linearization and discretization of system (29) produces:

$$\widetilde{\boldsymbol{x}}_{ST,k+1} = A_{ST}\widetilde{\boldsymbol{x}}_{ST,k} + B_{ST}\widetilde{\boldsymbol{u}}_{ST,k} + h_{ST} \tag{30}$$

being:

$$\widetilde{\boldsymbol{x}}_{ST,k} = \begin{bmatrix} V_{dc,ST,k} & \delta_{ST,k} & I_{dc,ST,k} \\ SOC_k & V_{ac,ST,k} & \sigma_{ST,k} & \omega_{f,ST,k} & m_{a,ST,k} \end{bmatrix}^{\mathrm{T}} \tag{31}$$

$$\widetilde{\boldsymbol{u}}_{ST,k} = \begin{bmatrix} \omega_{ST,k} & J_{ST,k} \end{bmatrix}^{\mathrm{T}}. \tag{32}$$

Expressions for the matrices involved in the above equations can be found in Appendix.

Additional constraints included in the ST MPC controller are listed in the following. The ST unit frequency does not have to exceed the minimum limit f_{min} and the maximum limit f_{max}, so:

$$2\pi f_{\min} \le \omega_{ST,k} \le 2\pi f_{\max}. \tag{33}$$

The modulation index is constrained in order to guarantee the inverter working in its operational range [33]:

$$m_{a,\min} \le m_{a,ST,k} \le m_{a,\max}. \tag{34}$$

The inverter capability curve can be linearized and discretized in order to impose:

$$\sqrt{P_{ac,ST,k}^2 + Q_{ST,k}^2} \le A_{ST} \tag{35}$$

A_{ST} being the ST inverter rating.

Finally, the ST must be in charge of the voltage control. Thus, regulation of the Storage AC side voltage $V_{ac,ST}$ is mandatory. As such voltage is not a state, it is necessary to express it as a function of the Storage states and inputs in order to obtain a linear constraint among them. Using the simplified voltage drop expression, one has:

$$V_{ac,ST} = \frac{m_{a,ST}V_{dc,ST}}{2\sqrt{2}} - \Delta v \tag{36}$$

$$\Delta v = \frac{1}{3V_{ac,ST}}\left(R_{f,ST}P_{ac,ST} + X_{f,ST}Q_{ST}\right). \tag{37}$$

So, the constraint for $V_{ac,ST}$ at time sample kT_s is:

$$-\varepsilon_V + V_{ac,ST}^{*} + \Delta v \le \frac{m_{a,ST,k}V_{DC,ST,k}}{2\sqrt{2}} \le \Delta v + V_{ac,ST}^{*} + \varepsilon_V \tag{38}$$

Where ε_V is half the amplitude of a boundary layer centered in $V_{ac,ST}^{*}$ where the Storage AC voltage must lay in. As for the other constraints, (38) has to be linearized. Please note that Δv is calculated as in starting from the measurements of voltage and active and reactive power at the beginning of the prediction horizon and then supposed to be constant until the following sampling instant.

So, defining:

$$\widetilde{\boldsymbol{u}}_{ref,ST,k} = \begin{bmatrix} 2\pi^{*}f_r & 0 \end{bmatrix}^{\mathrm{T}} \tag{39}$$

$$\widetilde{\boldsymbol{x}}_{ref,ST,k} = \begin{bmatrix} V_{dc,ref,ST,k} & \delta_{ref,ST,k} & I_{dc,ref,ST,k} & SOC_{ref,k} \\ V_{ac,ref,ST,k} & \sigma_{ref,ST,k} & \omega_{f,ref,ST,k} & m_{a,ref,ST,k} \end{bmatrix}^{\mathrm{T}} \tag{40}$$

and

$$\boldsymbol{e}_{ST,k} = \widetilde{\boldsymbol{x}}_{ref,ST,k} - \widetilde{\boldsymbol{x}}_{ST,k} \tag{41}$$

the ST MPC local controller has to solve the following optimization problem:

$$\begin{aligned} \min_{\boldsymbol{u}_{ST,k+i}} \quad & \boldsymbol{e}_{ST,k+N}^{T}Q\boldsymbol{e}_{ST,k+N} + \sum_{i=0}^{N-1}\Big\{\boldsymbol{e}_{ST,k+i|k}^{T}Q\boldsymbol{e}_{ST,k+i|k} \\ & + \left(\widetilde{\boldsymbol{u}}_{ST} - \widetilde{\boldsymbol{u}}_{ref,ST}\right)_{k+i}^{T}R\left(\widetilde{\boldsymbol{u}}_{ST} - \widetilde{\boldsymbol{u}}_{ref,ST}\right)_{k+i}\Big\} \end{aligned} \tag{42}$$

subject to: system predicted dynamics(30), bound on frequency (33) and on modulation index(34), voltage regulation (38) and capability curve (35).

Numerical values of the reference signals in (40) and of the weighting matrices Q and R depend on the operational mode of the controller (which will be clarified in the next section). The resulting control scheme is reported in Fig. 4 showing that the regulator relies only on local measurements.

3.2.1. Storage controller–normal operation

As specified before, in NO conditions the Storage must act as an independent voltage source; therefore, its only job is to close the active and reactive power balance (slack bus). It is then apparent that, in this operating mode, there are no reference values of the states to be tracked, which leads to define the following MPC controller matrices where the values of $R_{ST\text{-}NO}$ are chosen with the trial and error technique:

$$\begin{cases} Q = Q_{ST-NO} = diag(0_{1\times 8}) \\ R = R_{ST-NO} = diag\left(r_{\omega}^{ST}, r_{J}^{ST}\right) \end{cases} \tag{43}$$

3.2.2. Storage controller–power priority

In PP mode the Storage MPC controller forces the unit to exchange a fixed power to the grid, namely $P_{ab,lim}$. This is achieved as follows: consider the third of (29) at steady-state and multiply both members by $I_{dc,ST}$. It follows that:

$$\begin{aligned} & E(SOC)I_{dc,ST} - R_{ST}I_{dc,ST}^2 \\ & = V_{dc,ST}I_{dc,ST} \\ & = P_{ac,ST} \\ & = P_{ab,\lim} \end{aligned} \tag{44}$$

which gives:

$$V_{dc,ST}^2 - E(SOC)V_{dc,ST} - R_{ST}P_{ab,\lim} = 0. \tag{45}$$

The positive solution $V_{dc,ref,ST,k}$ of (45) is the reference value to which the Storage PP MPC controller regulates the DC link voltage. So, the corresponding weight must be activated, modifying the Storage control matrices, chosen with the trial and error technique, as follows:

$$\begin{cases} Q = Q_{ST-PP} = diag\left(q_{V_{dc}}^{ST}, 0_{1\times 7}\right) \\ R = R_{ST-PP} = diag\left(r_{\omega}^{ST}, r_{J}^{ST}\right) \end{cases}. \tag{46}$$

3.2.3. Storage controller–SOC priority

In case the Storage is absorbing power but its SOC becomes greater than a threshold SOC_{lim}, it enters the SP mode in which the MPC controller forces it to nullify its power injection. This is done as in the PP mode with the only difference that in SP model $P_{ab,lim}$ is set to 0. So, the Storage control matrices, chosen with the trial and error technique, in SP operational mode can be written as:

$$\begin{cases} Q = Q_{ST-SP} = diag\left(q_{V_{dc}}^{ST}, 0_{1\times 7}\right) \\ R = R_{ST-SP} = diag\left(r_{\omega}^{ST}, r_{J}^{ST}\right) \end{cases}. \tag{47}$$

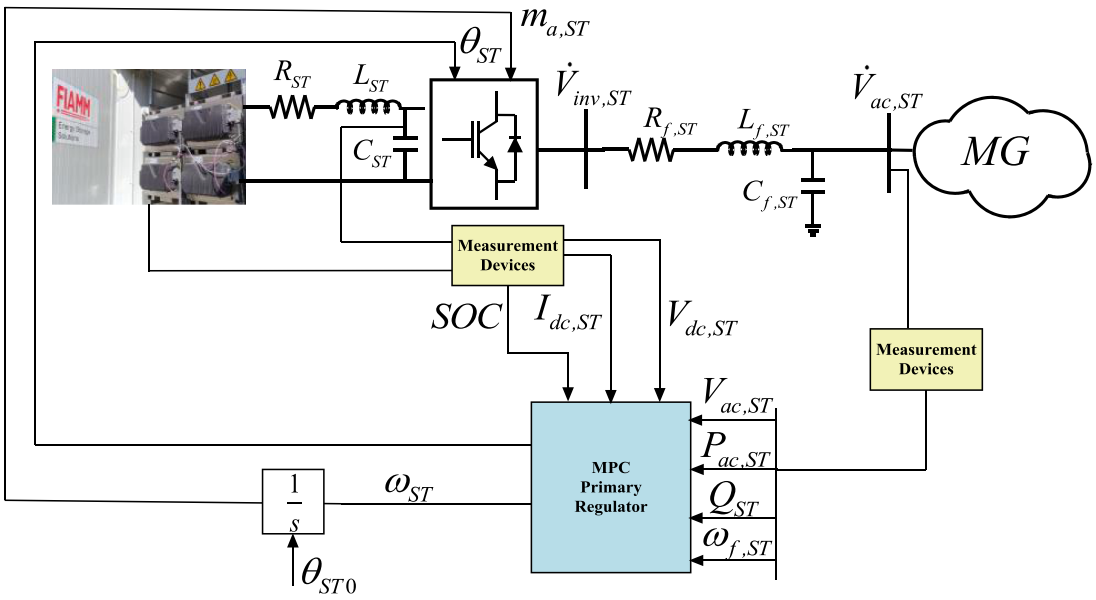

Fig. 4. Storage control scheme.

3.3. Automatic transition among operating modes

The transition of local unit controllers in accordance with the MG operational modes is easily performed by changing the MPC controllers weighting matrices Q and R. The aim of this subsection is to define the conditions for such transition. The Storage MPC controller transition from NO to PP occurs when the Storage is required to absorb a DC power $P_{dc,ST}$ in absolute value greater than a specified threshold $P_{ab,lim}$ sufficiently close to its maximum power absorption limit, namely $P_{dc,\max}$. So, with the adopted sign conventions, the condition for the transition of the Storage controller from the NO to PP is:

$$P_{dc,ST} < P_{ab,lim}. \tag{48}$$

Similarly, the Storage MPC controller switches from NO to SP when:

$$SOC > SOC_{lim} \tag{49}$$

SOC_{lim} being a specified threshold lower than 100%.

In both cases, the power injected by the PV units into the MG $P_{ac,PV}$ must decrease to satisfy the active power balance. As a consequence, since the PV controllers haven't produced any variation in the PV power yet, the DC link voltages increase (in accordance to (11)). At this point, each PV controller tries to reduce its local DC link voltage by increasing δ_{PV} (acting on ω_{PV}). The result is an increase of the angular frequency $\omega_{f,PV}$ measured at the PV terminals. So, the condition for the PV controller transition from NO to CURT is:

$$\omega_{f,PV} > 2\pi f_{curt} \tag{50}$$

$2\pi f_{curt}$ being a specified threshold. The inverse transition (from PP or SP to NO) occurs when the load request increases. In this case, since the PV units must guarantee the active power balance, they need to increase their real power injection. So, the condition for the PV controller transition from PP_SP to NO is:

$$P_{ac,PV} > kP_{PV,MPPT} \quad k \in (0,1) \tag{51}$$

where k is a suitable coefficient to improve the effectiveness of the controller transition.

At the same time, one can observe a decrease in the Storage AC-bus angular frequency $\omega_{f,ST}$ because the PP (or SP) Storage control acts to maintain the voltage set-point calculated from (45), decreasing the modulation angular frequency ω_{ST}. So, the condition for the Storage controller transition back to NO is:

$$\omega_{f,ST} < 2\pi f_{min,NO} \tag{52}$$

$f_{min,NO}$ being another specified threshold.

As a result, one can notice that the proposed controller provides an intrinsic frequency dynamic that allows managing the local unit controller in all the relevant MG operational assets without the need of ICT infrastructures or dedicated elements to emulate an inertial frequency response of the system. The logic described can be easily translated into the logic circuits depicted in Fig. 5 and Fig. 6 (one for each type of controller).

4. Simulations and results

The aim of this section is to validate the performance and proper operation of the proposed MPC based decentralized control approach described in Section 3. The first part of this section will describe the test case MG in detail. Following, several events (load and irradiance variations) shall be considered to evaluate the capabilities of the propose control architecture to provide an effective voltage and frequency regulation in all the discussed operating modes (i.e. NO, PP and SP). Finally, a comparison with a tradition decentralized approach for islanded MGs is proposed in order to highlight the main advantage of the proposed approach.

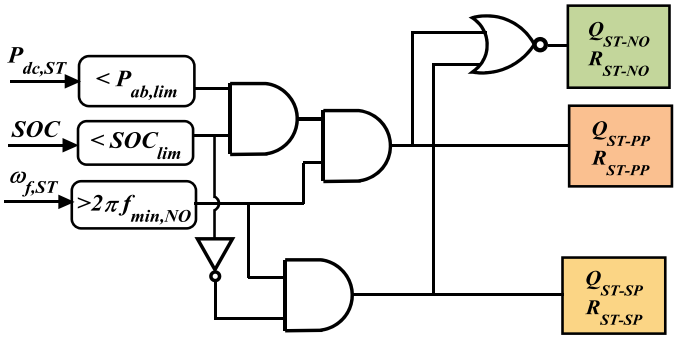

Fig. 5. Storage MPC controller logics transition circuit.

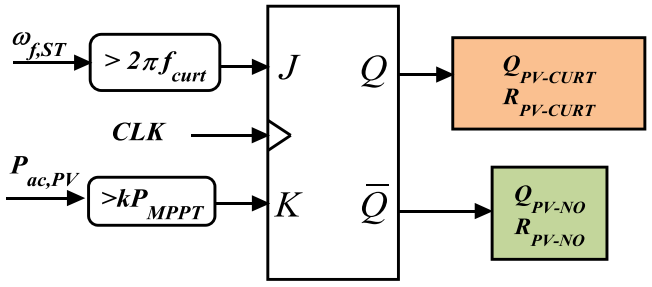

Fig. 6. PV MPC controller logics transition circuit.

4.1. Definition of the testcase MG layout and parameters

The proposed control system has been applied to the microgrid described in [31] and depicted in Fig. 7, consisting of two PV units and one Storage.

The peak powers of units PV1 and PV2 are respectively 16 kW and 80 kW while the corresponding inverter ratings are 17 kVA and 85 kVA. Transformer T-PV2 is at unitary transformation ratio. For the Storage the NCC is 228 Ah while power limits are 25 kW (when the Storage is charging) and 60 kW (when the Storage is discharging) and the inverter rating is 62 kVA. The load is connected at the MG common bus.

Simulation are performed in Simulink/Simscape® environment that represents all the MG components and infrastructure with a high level of detail. Inverters are two-level IGBT converters whose models are available in the Simscape library. Moreover, modulation is performed using a PWM technique with a 10 kHz carrier signal. PV units are modelled as suggested in [31], while details on the adopted Storage model can be found in [35]. Cables are modelled by means of resistive-inductive series impedances, while transformers are represented with the only leakage reactance. Numerical values of the sources and grid parameters appear in Tables 2 and 3 respectively.

All the simulations start from an initial working point where the PV units are both working at their MPP with an irradiance of 1 kW/m^2 producing respectively 16 kW and 80 kW at unitary power factor while the ST unit is regulating its terminal voltage at 230 V acting as a slack bus. The initial load is characterized by an R-L parallel impedance corresponding to 80 kW and 15 kVAr at the rated system voltage.

Table. 2
Sources parameters.

Parameter	Value	Parameter	Value	Parameter	Value
C_{PV}	3.3 mF	R_{ST}	1.12 Ω	C_{PV2}	6.0 mF
$R_{f,PV1}$	3.14 mΩ	L_{ST}	1 mH	$R_{f,PV2}$	1.05 mΩ
$L_{f,PV1}$	1 mH	$R_{f,ST}$	3.14 mΩ	$L_{f,PV2}$	0.3 mH
$C_{f,PV1}$	10 μF	$L_{f,ST}$	1 mH	$C_{f,PV2}$	5 μF
C_{ST}	3.5 mF	$C_{f,ST}$	10 μF	–	–

Table. 3
Grid Parameters.

Parameter	Value	Parameter	Value
T-PV2 $v_{cc\%}$	8%	T-PV2 A_n	85 kVA
$R_{c,PV1}$	0.15 Ω	$X_{c,PV1}$	3.28 mH
$R_{c,PV2}$	0.04 Ω	$X_{c,PV2}$	0.05 mH
$R_{c,ST}$	0.04 Ω	$X_{c,ST}$	0.03 mH

The sampling time T_s for the MPC controllers is set to 1 ms while the time horizon N is equal to 3. An experimental application of an MPC controller for the storage NO mode, with this controller parameter setting is reported in [36]. For the sake of completeness, all regulators parameters introduced in Section 3 are reported in Tables 4 and 5.

4.2. Simulation A – load and irradiance variation in NO

The aim of this simulation is to show the performances of the NO controllers in case of two contingencies: *i)* a load decreasing from 80 kW to 70 kW happening at 0.2 s and *ii)* a solar irradiance ramp decreasing starting at 0.6 s and passing from 1 kW/m^2 to 0.7 kW/m^2 in 0.2 s.

Table. 4
PV controllers parameters.

f_{min}/f_{max}	49.5/50.5 Hz	ε_Q	1 kVAr	r_{ω}^{PV}	700
$m_{a,\min}$	0.5	f_{curt}	50.3 Hz	r_J^{PV}	200
$m_{a,\max}$	1.05	k	0.9	$q_{V_{dc}}^{PV}$	60

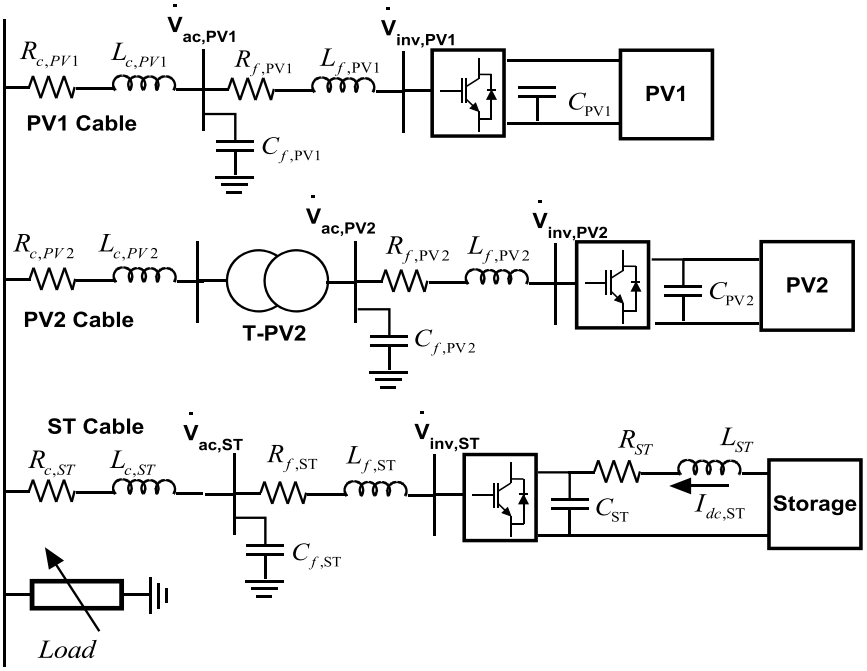

Fig. 7. One-line diagram of test case MG.

Table. 5
Storage controller parameters.

f_{min}/f_{max}	49.5/50.5 Hz	ϵ_V	11.5 V (5%)	$q^{ST}_{V_{dc}}$	10
$m_{a,\min}$	0.5	$P_{ab,lim}$	−20 kW (PP)	r^{ST}_{J}	30
$m_{a,\max}$	1.05		0 kW (SP)	r^{ST}_{ω}	10
$f_{min,NO}$	49.8 Hz	SOC_{lim}	90.0%	–	–

As far as the load reduction occurs, the controllers make the storage change its power absorption in order to close the power balance while PV units, after a quick transient, return to their MPP production (as one can see from Fig. 8).

When the irradiance reduction occurs, the ST unit behaves in the opposite way, thus increasing its power production passing from charging to discharging mode, in order to cope with the PV units power decreasing.

During these events, the DG units AC voltages (depicted in Fig. 9) are kept between admissible ranges (i.e. 230 ± 5% V, dash-dotted black lines in Fig. 9).

Finally it is important to analyze the system frequency behavior, reported in Fig. 10, where one can notice that the frequency transient after the contingency is restored to the desired value of 50 Hz at the end of the transient.

For the sake of completeness, Fig. 11 reports the modulation index requests provided by the controllers to each DG unit in order to highlight the achievement of the local MPC controller constraints and the feasibility of the obtained control laws.

As a conclusion, this set of simulation pointed out that the proposed control architecture is capable to ensure the system power balance restoring the system frequency at 50 Hz in NO with a proper control action on the system voltages.

4.3. Simulation B– load decrease causing PP operation

The aim of this second simulation is to test the performances of the proposed controllers in PP mode. This is done by imposing a load decrease from the initial value of 80 kW to 25 kW at 0.2 s. As one can see form Fig. 12, such a relevant load variation causes the ST absorption to exceed the 20 kW limit implemented in the local MPC controller that triggers the PP mode. Following, at 0.6 s the load is increased in order to restore a NO condition; this tests the NO/PP transition in both directions.

The active power dynamics of load and DG units is reported in Fig. 12 where it is possible to notice that consequently to the load negative step, the storage provides it maximum absorbing power, equal to 25 kW. Since the ST limit power $P_{ab,lim} = 20$ kW is exceeded, the local ST unit controller transition to PP mode is triggered in accordance to the scheme of Fig. 5 with a consequent regulation of active power to 20 kW.

As far as PV units are concerned, when the system frequency (reported in Fig. 13) locally measured at each PV units terminals exceeds the value f_{curt} (50.3 Hz in this simulation), the local PV controllers switch

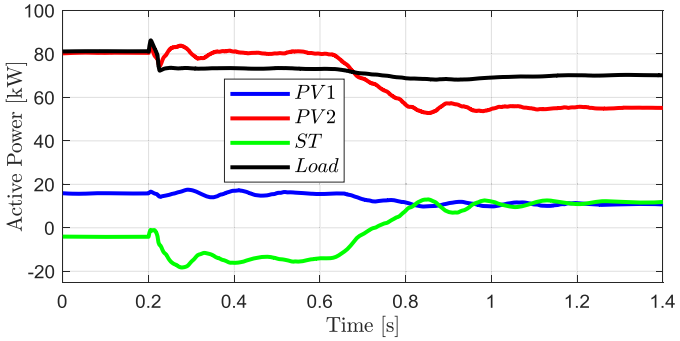

Fig. 8. Active powers time profiles.

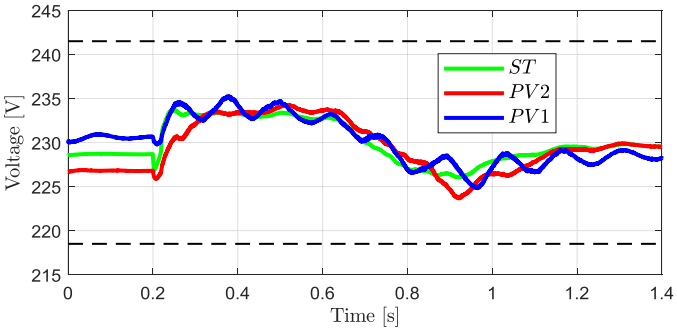

Fig. 9. RMS phase-to-ground voltage time profiles.

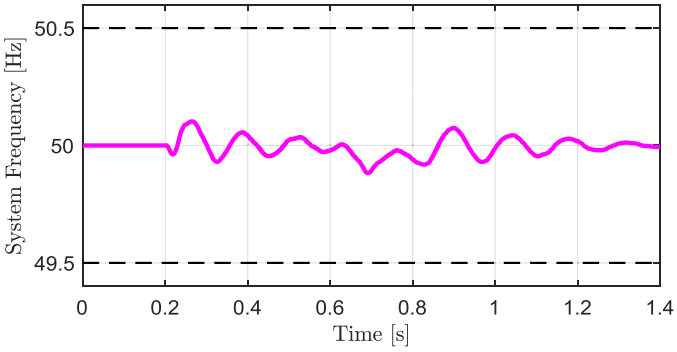

Fig. 10. System frequency time profiles.

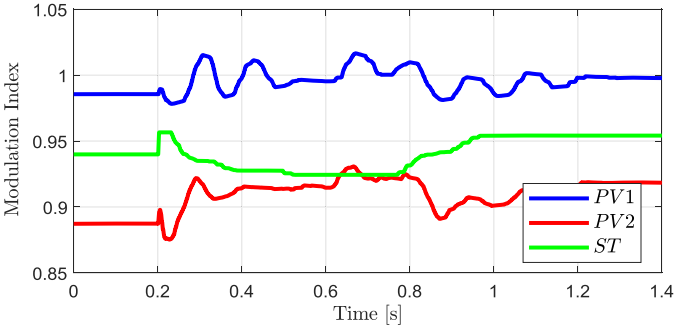

Fig. 11. DG units modulation index time profiles.

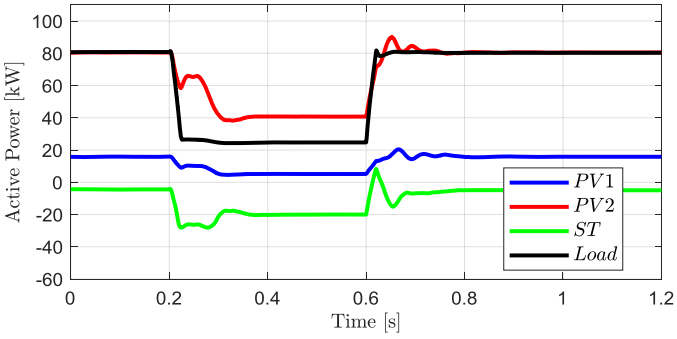

Fig. 12. Active powers time profiles.

to CURT mode and the PV units are forced to curtail their production. As a result, one can see from Fig. 12 that after a very quick transient the ST power absorption is taken to 20 kW while PV units are suitably curtailed. Moreover, the system frequency is properly restored to its rated value of

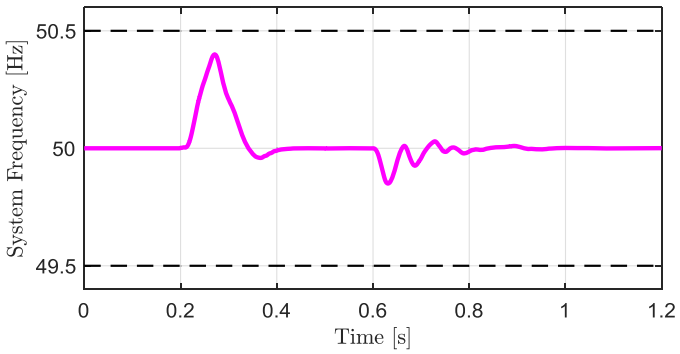

Fig. 13. Frequency time profiles.

50 Hz within 0.2 s achieving the goal of the secondary regulation.

Finally, the last part of the simulation points out how the system is automatically capable of restoring the initial NO operational mode when the load increases always providing a final frequency of the system equal to 50 Hz.

Fig. 14 reports the DG unit voltages during the whole transient. From this figure one can notice that the proposed MPC decentralized controllers are capable to keep the system voltages within their admissible ranges also when the ST unit switches to PP mode.

Fig. 15 shows the DC link voltages of the three sources highlighting that the first transition needs about 0.1 s, while the NO restoration occurs in about 0.2 s. Moreover, one can also notice that PV units are taken back to their initial DC voltage value (i.e. the MPP one) when the NO mode is restored.

As a conclusion one can state that the proposed control approach provides a suitable transition of the local controller in case of saturation of the storage active power without communication between converters. Moreover, the system frequency is restored after each transient to its rated value without any secondary regulation.

4.4. Simulation C – load decrease causing SP operation

The aim of this third simulation is to show the performance of the proposed control strategy in the SP mode. To better highlight this, the ST *SOC* is initialized very close to SOC_{lim} due to the very slow dynamics of the SOC with respect to the frame of the proposed simulation. From this initial condition, a load power decreasing from 80 kW to 40 kW at 0.2 s is considered. This load variation implies first the transition to the PP mode followed by SP mode when the SOC reaches its maximum value.

After the first instants after the load variation, the storage increases its power absorption until reaching its maximum value (25 kW). As for the simulation of Section B, this causes the activation of PP mode for the ST and CURT for the PV units (Fig. 16).

Following this transient the SOC overcome its limit value at 0.5 s (see Fig. 17), causing the transition to SP mode for the ST controller in accordance to the proposed transition logic. This results in the zeroing of

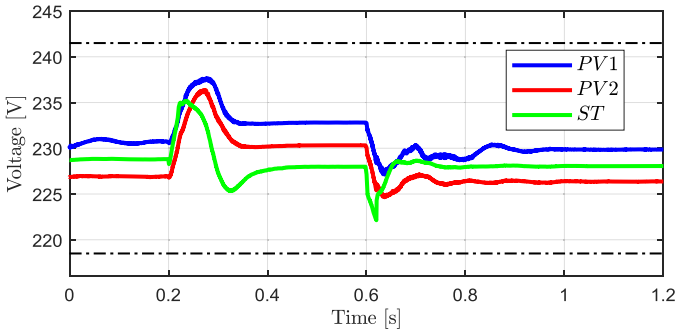

Fig. 14. RMS values of phase to ground voltages.

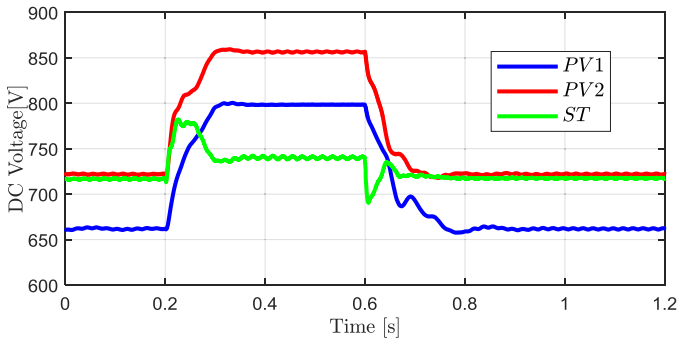

Fig. 15. DC-link voltage time profiles.

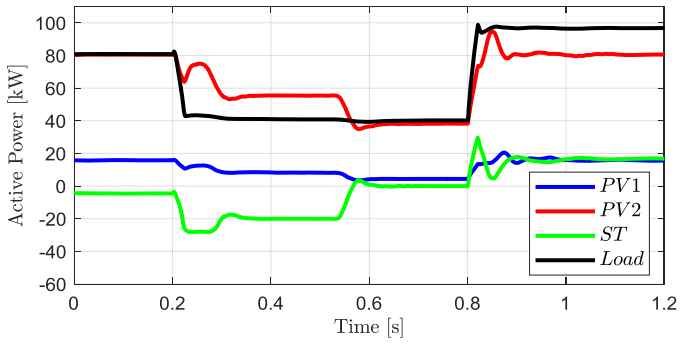

Fig. 16. Active powers time profiles.

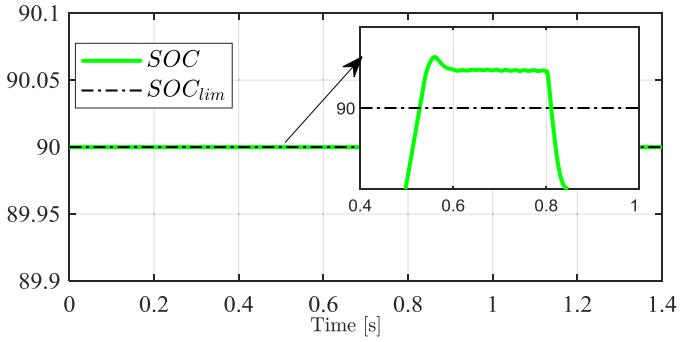

Fig. 17. Storage SOC time profile.

the power absorbed by the battery, as one can see from Fig. 16 at 0.5 s. In this condition PV units further curtail their production in order to satisfy the MG power balance. Finally, the simulation highlights how NO condition is suitably restored for all DERs when the load increases.

Once again, the effectiveness of the proposed decentralized control architecture in restoring the system frequency without any need of communication between DG units controllers is shown in Fig. 18.

Finally, it is also important to highlight the achievement of voltage regulation in all operation modes, as depicted in Fig. 19 for AC unit voltages and in Fig. 20 for DC voltages. This highlights the effectiveness of the proposed control architecture to restore MPP voltage after the CURT operational modes of the PV units.

Also in this third scenario the proposed MPC control approach provides an effective regulation in terms of power balance, frequency restoration and voltage control in case of saturation of the storage SOC without any communication between DG units.

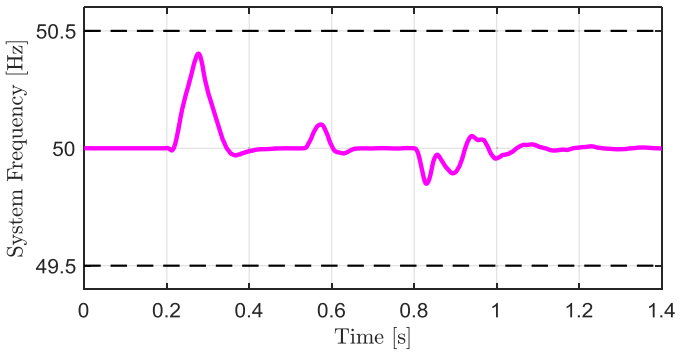

Fig. 18. Frequency time profiles.

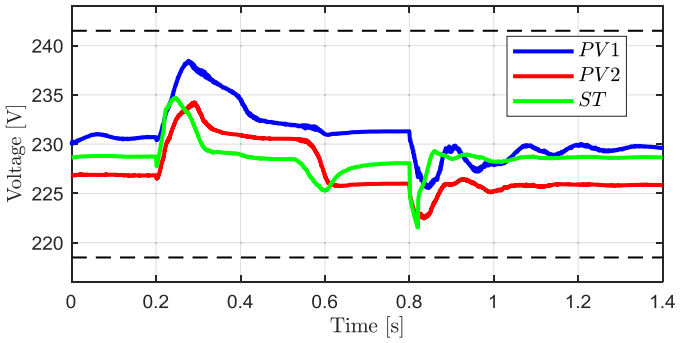

Fig. 19. RMS values of phase to ground voltages.

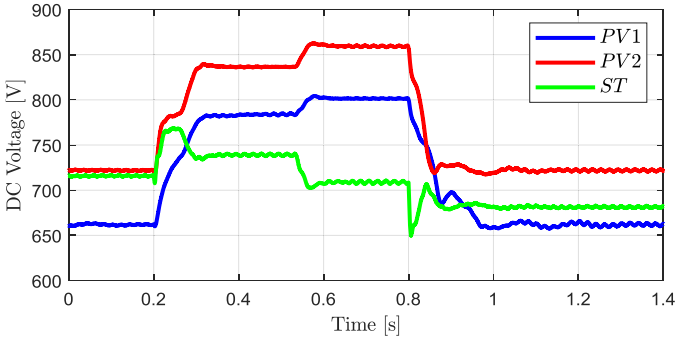

Fig. 20. DC-link voltage time profiles.

4.5. Comparison with a tradition decentralized approach for islanded MGs

In order to better highlight the improvements provided by the proposed decentralized MPC controllers architecture a dedicated comparison with a transition droop-based approach is provided [15]. The ST unit controls its AC terminal voltage implementing a droop characteristic for its frequency (droop coefficient equal to 0.05 Hz/MW). The ST controller accounts for inner voltage and current loops implemented as traditional Proportional-Integral (PI) controllers [37]. PV units work as active and reactive power sources thanks to the inner current control loop, but also accounting for the possibility of curtailing their active power reference in accordance to the system frequency variation (Limited Frequency Sensitive Mode – Over-frequency [38]). The PV Power curtailment characteristic is depicted in Fig. 21.

4.5.1. Load decreasing in NO

In this simulation the same load decreasing provided in SubSection 4.1. is considered, i.e. passing from 80 kW to 70 kW at 0.2 s

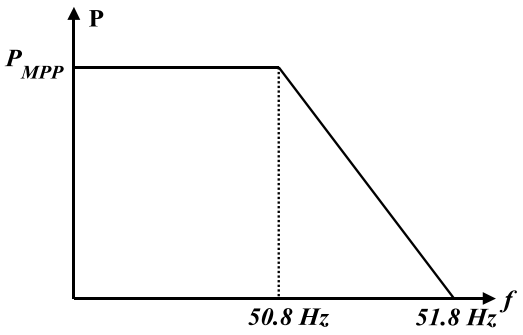

Fig. 21. PV units power curtailment characteristic for the traditional control.

corresponding to the system NO.

As one can notice from Fig. 22 the performances of the MPC and traditional approach are very similar. The MPC controller provides some oscillation in the PV power production; on the other hand, a smother behavior of the ST unit is appreciated. Also the system voltages for both cases are characterized by good dynamic and steady-state values as shown in Fig. 23. Moreover, it is possible to notice that the voltages dynamic with the proposed MPC controllers has more oscillations for the PV units. However, oscillations have a limited excursion (roughly 2%) and are almost completely damped in 0.5 s.

In NO, the main advantage of the proposed approach with respect to the traditional droop-based one is in the system frequency behavior (Fig. 24). As one can notice, the frequency transient is much smaller, and the final system frequency is restored at 50 Hz avoiding the need of a secondary regulation.

4.5.2. Load decreasing in PP

This second simulation provides a comparison between the proposed MPC decentralized control architecture and the traditional droop-based one after a higher load decreasing, passing from 80 kW to 20 kW at 0.2 s, causing the transition to PP mode.

As one can see from Fig. 25, the traditional approach provides a regulation of the power in the final steady state thanks to the suitable setting of the droop characteristic. However, in the first part of the transient, the converter maximum power is exceeded and this might be a dangerous situation causing the trip of the converter protection. The MPC controller, on the other hand, provide a control on the ST power and thus provide a faster limitation that prevent from this dangerous overloading.

The system voltages are suitable for both the proposed control approaches as pointed out in Fig. 26. The optimal performances of the proposed MPC decentralized control architecture on the system frequency can be appreciated in Fig. 27, where, after a very fast transient, it is restored at its rated value.

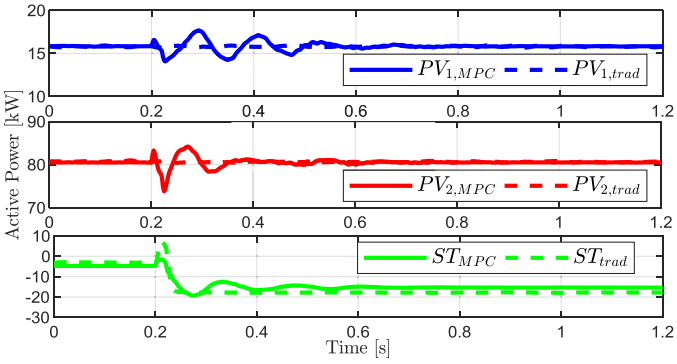

Fig. 22. Active powers time profiles.

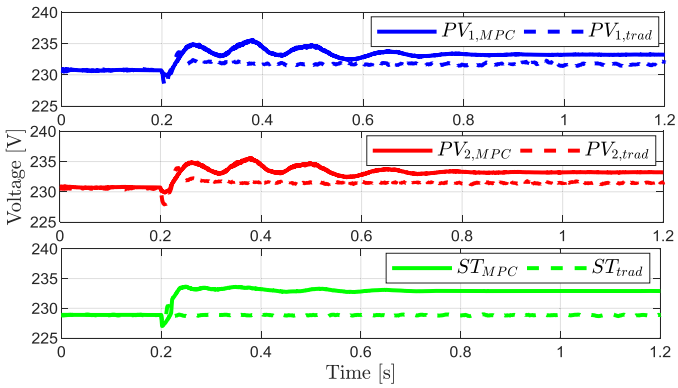

Fig. 23. RMS values of phase to ground voltages.

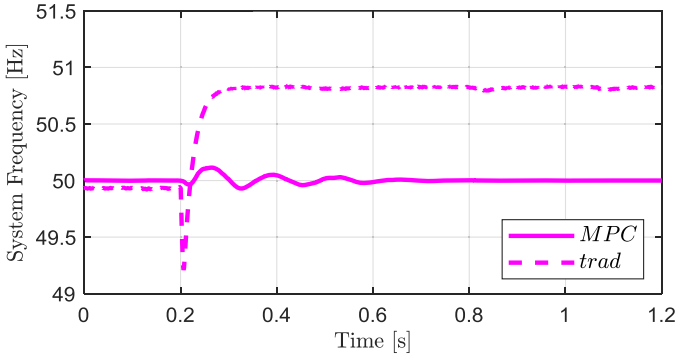

Fig. 24. Frequency time profiles.

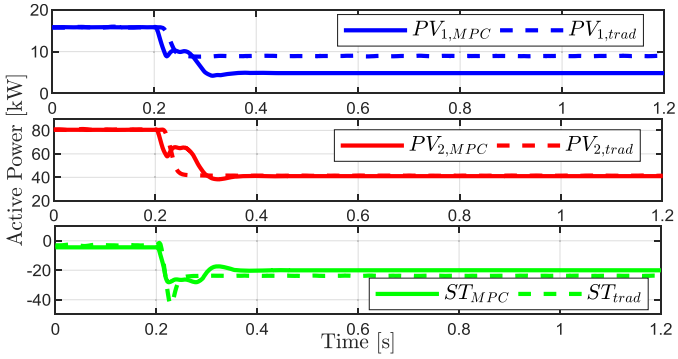

Fig. 25. Active powers time profiles.

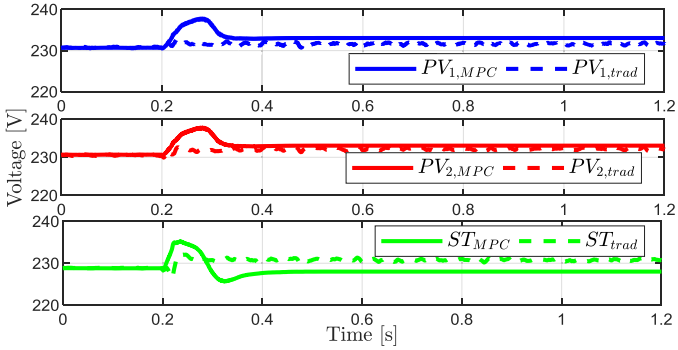

Fig. 26. RMS values of phase to ground voltages.

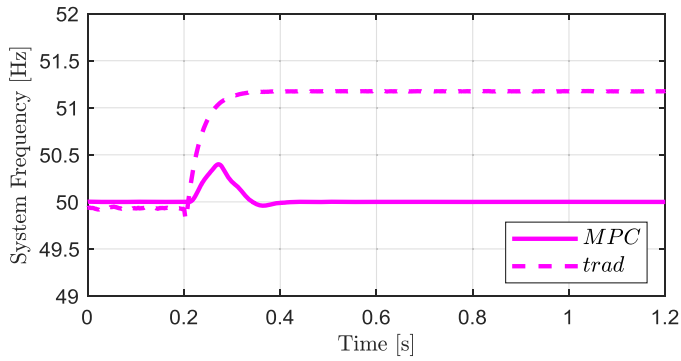

Fig. 27. Frequency time profiles.

5. Conclusions

This paper proposed a new control strategy for islanded PV-Storage MGs based on decentralized MPC controllers architecture that properly manage the MG under all its operational assets. Three different operating conditions were defined for the for islanded PV-Storage MG (namely NO, PP and SP) and conditions to automatically switch from one mode to the others were derived.

The main goal of the proposed approach was that of achieving a proper operation of an islanded PV-Storage MG in terms of frequency and voltage regulation without communication between the MG DG units. In order to do that, a suitable triggering logic for each local controller was designed based only on local controller measurements.

Simulations to validate the performances and the robustness of the proposed control approach were performed in Simulink/Simscape® environment on a realistic test-case MG. Results highlighted the effectiveness of the proposed control architecture to achieve power balance, voltage regulation and frequency regulation in all the considered operational modes. Moreover, simulations highlighted how the proposed approach is capable to achieve the goals of both primary and secondary frequency regulation, that is not possible with state-of-the-art decentralized controllers that implements a communication-based centralized approach to restore the MG system frequency (secondary frequency regulation).

Future developments shall cover two different areas. From a theoretical point of view, a deeper investigation on the system stability will be conducted that should in turn give the possibility of defining analytical or semi analytical criteria for setting the controller parameters. Moreover, robustness of the controllers with respect to both parametric uncertainties and errors introduced by the linearization of the system at each MPC run will be analyzed in detail. On the application side, one will look for an improvement of the voltage/reactive power control performances of the proposed approach; furthermore, an experimental validation of the simulative results in a Rapid-Control-Prototyping set-up with real power components will be proposed.

Declaration of Competing Interest

The authors declare that they have no known competing financial interests or personal relationships that could have appeared to influence the work reported in this paper.

Appendix: Derivation of the equations for the optimization problem in the PV and storage controllers

The aim of this Appendix is to provide all the details necessary to transform system (13) into (16) for the PV units and system (29) into (30) for the storage one. Let us start with the PV and follow the steps identified in Section 3.1 after Eq. (15).

System Linearization

Since linearization is necessary at each MPC sample time, at this stage, for the sake of generality, one indicates with subscript 0 the value assumed by all quantities in the instant t_0 around which the linearization is performed. So, (14) becomes:

$$\begin{bmatrix} \dot{V}_{dc,PV} \\ \dot{\delta}_{PV} \end{bmatrix} = A_{C,PV,t_0} \begin{bmatrix} V_{dc,PV} \\ \delta_{PV} \end{bmatrix} + B_{C,PV,t_0} \begin{bmatrix} m_{a,PV} \\ \omega_{PV} \end{bmatrix} + C_{C,PV,t_0} \begin{bmatrix} V_{ac,PV} \\ \sigma_{PV} \\ \alpha \\ T \\ \omega_{f,PV} \end{bmatrix} + D_{C,PV,t_0} \tag{A.1}$$

where:

$$\begin{aligned}
A_{C,PV,t_0} &= \begin{bmatrix} \frac{1}{C_{PV}} \frac{\partial I_{PV}(V_{dc,PV},\alpha,T)}{\partial V_{dc,PV}}\Big|_{t=t_0} & -\frac{3m_{a,PV,0}V_{ac,PV,0}}{2\sqrt{2}x_{f,PV}C_{PV}}\cos(\sigma_{PV,0}+\delta_{PV,0}) \\ 0 & 0 \end{bmatrix} \\
B_{C,PV} &= \begin{bmatrix} -\frac{3V_{ac,PV,0}}{2}\sin(\sigma_{PV,0}+\delta_{PV,0}) & 0 \\ 0 & 1 \end{bmatrix} \\
C_{C,PV,t_0} &= \begin{bmatrix} -\frac{3m_{a,PV,0}}{2\sqrt{2}x_{f,PV}C_{PV}}\sin(\sigma_{PV,0}+\delta_{PV,0}) & -\frac{3m_{a,PV,0}V_{ac,PV,O}}{2\sqrt{2}x_{f,PV}C_{PV}}\cos(\sigma_{PV,0}+\delta_{PV,0}) & \frac{1}{C_{PV}}\frac{\partial I_{PV}(V_{dc,PV},\alpha,T)}{\partial \alpha}\Big|_{t=t_0} & \frac{1}{C_{PV}}\frac{\partial I_{PV}(V_{dc,PV},\alpha,T)}{\partial T}\Big|_{t=t_0} & 0 \\ 0 & 0 & 0 & 0 & -1 \end{bmatrix} \\
D_{C,PV,t_0} &= \begin{bmatrix} \frac{3m_{a,PV,0}V_{ac,PV,0}}{2\sqrt{2}x_{f,PV}C_{PV}}\left[\sin(\sigma_{PV,0}+\delta_{PV,0}) + (\sigma_{PV,0}+\delta_{PV,0})\cos(\sigma_{PV,0}+\delta_{PV,0})\right] \\ +\frac{1}{C_{PV}}\left[\frac{\partial I_{PV}(V_{dc,PV},\alpha,T)}{\partial T}\Big|_{t=t_0} - \frac{\partial I_{PV}(V_{dc,PV},\alpha,T)}{\partial V_{dc,PV}}\Big|_{t=t_0} - \frac{\partial I_{PV}(V_{dc,PV},\alpha,T)}{\partial \alpha}\Big|_{t=t_0} - \frac{\partial I_{PV}(V_{dc,PV},\alpha,T)}{\partial T}\Big|_{t=t_0}\right] \\ 0 \end{bmatrix}
\end{aligned} \tag{A.2}$$

Discretization

Supposing to sample all quantities with sampling time T_s, approximating all time derivatives with the Euler backward method i.e. for any quantity x

$$\dot{x}(kT_s) \cong \frac{x((k+1)T_s) - x(kT_s)}{T_s} \tag{A.3}$$
$$k = 1..N-1$$

N being the prediction horizon) and indicating with x_k the value assumed by variable x in $t{=}T_s$, one gets that:

$$\begin{bmatrix} V_{dc,PV,k+1} \\ \delta_{PV,k+1} \end{bmatrix} = (I_2 + T_s A_{C,PV,T_s}) \begin{bmatrix} V_{dc,PV,k} \\ \delta_{PV,k} \end{bmatrix} + T_s B_{C,PV,T_s} \begin{bmatrix} m_{a,PV,k} \\ \omega_{PV,k} \end{bmatrix} + T_s C_{C,PV,T_s} \begin{bmatrix} V_{ac,PV,k} \\ \sigma_{PV,k} \\ \alpha_k \\ T_k \\ \omega_{f,PV,k} \end{bmatrix} + T_s D_{C,PV,T_s} \tag{A.4}$$

I_n being the Identity matrix of order n.

Transformation of measures g_{PV} *into new states with no dynamics*

Since the time evolution of measurements is unknown during the prediction, they are supposed to remain constant overall a single prediction horizon and then updated at the following sampling instant, which corresponds to set:

$$\boldsymbol{g}_{PV,k+1} = \boldsymbol{g}_{PV,k}. \tag{A.5}$$

This allows to transform all components of $\boldsymbol{g_{PV}}$ into new states, which leads (A.4) to:

$$\begin{bmatrix} V_{dc,PV,k+1} \\ \delta_{PV,k+1} \\ V_{ac,PV,k+1} \\ \sigma_{PV,k+1} \\ \alpha_{,k+1} \\ T_{,k+1} \\ \omega_{f,PV,k+1} \end{bmatrix} = \begin{bmatrix} I_2 + T_s A_{C,PV,T_s} & T_s C_{C,PV,T_s} \\ 0_{5x2} & I_5 \end{bmatrix} \begin{bmatrix} V_{dc,PV,k} \\ \delta_{PV,k} \\ V_{ac,PV,k} \\ \sigma_{PV,k} \\ \alpha_{,k} \\ T_{,k} \\ \omega_{f,PV,k} \end{bmatrix} + \begin{bmatrix} T_s B_{C,PV,T_s} \\ 0_{5x2} \end{bmatrix} \begin{bmatrix} m_{a,PV,k} \\ \omega_{PV,k} \end{bmatrix} + \begin{bmatrix} T_s D_{C,PV,T_s} \\ 0_{5x1} \end{bmatrix} \tag{A.6}$$

Introduction of the time derivative of the modulation index as new auxiliary input

As it is important that the modulation index is constant at steady state no matter the value it assumes in its operational range, the following state equation can be added:

$$m_{a,PV,k+1} = m_{a,PV,k} + T_s J_{PV,k} \tag{A.7}$$

that transforms the modulation index in a state considering its derivative J_{PV} as an input, to be regulated to zero. This leads (A.7) to:

$$\begin{bmatrix} V_{dc,PV,k+1} \\ \delta_{PV,k+1} \\ V_{ac,PV,k+1} \\ \sigma_{PV,k+1} \\ \alpha_{,k+1} \\ T_{,k+1} \\ \omega_{f,PV,k+1} \\ m_{a,PV,k+1} \end{bmatrix} = \begin{bmatrix} I_2 + T_s A_{C,PV,T_s} & T_s C_{C,PV,T_s} & T_s B_{m_a,PV,T_s} \\ 0_{5x2} & I_5 & 0_{5x1} \\ 0_{1x2} & 0_{1x5} & 1 \end{bmatrix} \begin{bmatrix} V_{dc,PV,k} \\ \delta_{PV,k} \\ V_{ac,PV,k} \\ \sigma_{PV,k} \\ \alpha_{,k} \\ T_{,k} \\ \omega_{f,PV,k} \\ m_{a,PV,k} \end{bmatrix} + \begin{bmatrix} 0 & 0 \\ 1 & 0 \\ 0 & 0 \\ 0 & 0 \\ 0 & 0 \\ 0 & 0 \\ 0 & 0 \\ 0 & T_s \end{bmatrix} \begin{bmatrix} \omega_{PV,k} \\ J_{PV,k} \end{bmatrix} + \begin{bmatrix} T_s D_{C,PV,T_s} \\ 0_{6x1} \end{bmatrix} \tag{A.8}$$

where

$$B_{m_a,PV,T_s} = \begin{bmatrix} B_{C,PV,T_s}(1,1) \\ B_{C,PV,T_s}(2,1) \end{bmatrix} \tag{A.9}$$

which can be put in the form of (16)-(17)-(18) if one poses:

$$A_{PV} = \begin{bmatrix} I_2 + T_s A_{C,PV,T_s} & T_s C_{C,PV,T_s} & T_s B_{m_a,PV,T_s} \\ 0_{5x2} & I_5 & 0_{5x1} \\ 0_{1x2} & 0_{1x5} & 1 \end{bmatrix} \tag{A.10}$$

$$B_{PV} = \begin{bmatrix} 0 & 0 \\ 1 & 0 \\ 0 & 0 \\ 0 & 0 \\ 0 & 0 \\ 0 & 0 \\ 0 & 0 \\ 0 & T_s \end{bmatrix} \tag{A.11}$$

and

$$h_{PV} = \begin{bmatrix} T_s D_{C,PV,T_s} \\ 0_{6x1} \end{bmatrix} \tag{A.12}$$

The same way one can construct the matrices for the ST controller (30), whose final expression is:

$$A_{ST} = \begin{bmatrix} I_4 + T_s A_{C,ST,T_s} & T_s C_{C,ST,T_s} & T_s B_{m_a,ST,T_s} \\ 0_{3x4} & I_3 & 0_{3x1} \\ 0_{1x4} & 0_{1x3} & 1 \end{bmatrix} \tag{A.13}$$

$$B_{ST} = \begin{bmatrix} 0 & 0 \\ 1 & 0 \\ 0 & 0 \\ 0 & 0 \\ 0 & 0 \\ 0 & 0 \\ 0 & 0 \\ 0 & T_s \end{bmatrix} \tag{A.14}$$

and

$$h_{ST} = \begin{bmatrix} T_s D_{C,ST,t_0} \\ 0_{4\times1} \end{bmatrix} \tag{A.15}$$

Where:

$$A_{C,ST,t_0} = \begin{bmatrix} 0 & -\frac{3m_{a,ST,0}V_{AC,ST,0}}{\sqrt{8}x_{f,ST}C_{ST}}\cos\left(\sigma_{ST,0}+\delta_{ST,0}\right) & \frac{1}{C_{ST}} & 0 \\ 0 & 0 & 0 & 0 \\ -\frac{1}{L_{ST}} & 0 & -\frac{R_{ST}}{L_{ST}} & \frac{1}{L_{ST}}\frac{dE}{dSOC}\Big|_{t=t_0} \\ 0 & 0 & -\frac{1}{NCC} & 0 \end{bmatrix} \tag{A.16}$$

$$B_{C,ST,t_0} = \begin{bmatrix} -\frac{3V_{AC,ST,0}}{\sqrt{8}x_{f,ST}C_{ST}}\sin\left(\sigma_{ST,0}+\delta_{ST,0}\right) & 0 \\ 0 & 1 \\ 0 & 0 \\ 0 & 0 \end{bmatrix} \tag{A.17}$$

$$C_{C,ST,t_0} = \begin{bmatrix} -\frac{3m_{a,ST,0}}{\sqrt{8}x_{f,ST}C_{ST}}\sin\left(\sigma_{ST,0}+\delta_{ST,0}\right) & -\frac{3m_{a,ST,0}V_{AC,ST,0}}{\sqrt{8}x_{f,ST}C_{ST}}\cos\left(\sigma_{ST,0}+\delta_{ST,0}\right) & 0 \\ 0 & 0 & -1 \\ 0 & 0 & 0 \\ 0 & 0 & 0 \end{bmatrix} \tag{A.18}$$

$$D_{C,ST,t_0} = \begin{bmatrix} \frac{3m_{a,ST}V_{AC,ST,0}}{\sqrt{8}x_{f,ST}C_{ST}}\left[\sin\left(\sigma_{ST,0}+\delta_{ST,0}\right)+\left(\sigma_{ST,0}+\delta_{ST,0}\right)\cos\left(\sigma_{ST,0}+\delta_{ST,0}\right)\right] \\ 0 \\ \frac{1}{L_{ST}}\left(E(SOC_0)-\frac{dE}{dSOC}\Big|_{t=t_0}SOC_0\right) \\ 0 \end{bmatrix} \tag{A.19}$$

References

[1] P.G. Bueno, J.C. Hernández, F.J. Ruiz-Rodriguez, Stability assessment for transmission systems with large utility-scale photovoltaic units, IET Renew Power Gener 10 (5) (2016) 584–597.

[2] J.C. Hernández, F. Sanchez-Sutil, P. Vidal, C. Rus-Casas, Primary frequency control and dynamic grid support for vehicle-to-grid in transmission systems, Int J Electr Power Energy Syst 100 (2018) 152–166.

[3] J.C. Hernandez, P.G. Bueno, F. Sanchez-Sutil, Enhanced utility-scale photovoltaic units with frequency support functions and dynamic grid support for transmission systems, IET Renew Power Gener 11 (3) (2017) 361–372.

[4] "GOFLEX. Accessed: 2019-10-10. Generalized operational FLEXi- bility for Integrating Renewables in the Distribution Grid. https: //goflex-project.eu," in ed.

[5] "MERLON EU PROJECT " https://www.merlon-project.eu/" last accessed 2019-10-10," ed.

[6] K. Adam, M. Müller-Mienack, M. Paun, G. Sanchis, K. Strunz, e-HIGHWAY 2050—The ENTSO-E facilitated study programme towards a modular development plan on pan-European Electricity Highways System 2050, in: 2012 IEEE Power and Energy Society General Meeting, IEEE, 2012, pp. 1–6.

[7] H. Jiayi, J. Chuanwen, X. Rong, A review on distributed energy resources and MicroGrid, Renew Sustain Energy Rev 12 (9) (2008) 2472–2483, https://doi.org/10.1016/j.rser.2007.06.004. /12/01/ 2008.

[8] Y. Ghiassi-Farrokhfal, F. Kazhamiaka, C. Rosenberg, S. Keshav, Optimal design of solar PV farms with storage, IEEE Trans Sustain Energy 6 (4) (2015) 1586–1593, https://doi.org/10.1109/TSTE.2015.2456752.

[9] I. Bendato, Design criteria for the optimal sizing of integrated photovoltaic-storage systems, Energy 149 (2018) 505–515, https://doi.org/10.1016/j.energy.2018.02.056. /04/15/ 2018.

[10] K. Sun, L. Zhang, Y. Xing, J.M. Guerrero, A distributed control strategy based on DC bus signaling for modular photovoltaic generation systems with battery energy storage, IEEE Trans Power Electroni 26 (10) (2011) 3032–3045, https://doi.org/10.1109/TPEL.2011.2127488.

[11] H. Han, X. Hou, J. Yang, J. Wu, M. Su, J.M. Guerrero, Review of power sharing control strategies for islanding operation of AC Microgrids, IEEE Trans Smart Grid 7 (1) (2016) 200–215, https://doi.org/10.1109/TSG.2015.2434849.

[12] T. Vandoorn, J. De Kooning, B. Meersman, L. Vandevelde, Review of primary control strategies for islanded microgrids with power-electronic interfaces, Renew Sustain Energy Rev 19 (2013) 613–628.

[13] A. Mortezaei, M.G. Simões, M. Savaghebi, J.M. Guerrero, A. Al-Durra, Cooperative control of multi-master–slave islanded microgrid with power quality enhancement based on conservative power theory, IEEE Trans Smart Grid 9 (4) (2018) 2964–2975, https://doi.org/10.1109/TSG.2016.2623673.

[14] S. Peyghami, H. Mokhtari, P.C. Loh, P. Davari, F. Blaabjerg, Distributed primary and secondary power sharing in a droop-controlled LVDC microgrid with merged AC and DC characteristics, IEEE Trans Smart Grid 9 (3) (2018) 2284–2294, https://doi.org/10.1109/TSG.2016.2609853.

[15] J. Rocabert, A. Luna, F. Blaabjerg, P. Rodriguez, Control of power converters in AC microgrids, IEEE Trans Power Electron 27 (11) (2012) 4734–4749.

[16] N. Hatziargyriou, Microgrids: Architectures and Control, John Wiley & Sons, 2014.

[17] S. Adhikari, F. Li, Coordinated V-f and P-Q control of solar photovoltaic generators with MPPT and battery storage in microgrids, IEEE Trans Smart Grid 5 (3) (2014) 1270–1281, https://doi.org/10.1109/TSG.2014.2301157.

[18] M. Mao, C. Qian, Y. Ding, Decentralized coordination power control for islanding microgrid based on PV/BES-VSG, CPSS Trans Power Electron Appl 3 (1) (2018) 14–24, https://doi.org/10.24295/CPSSTPEA.2018.00002.

[19] H. Mahmood, D. Michaelson, J. Jiang, Decentralized power management of a PV/Battery hybrid unit in a droop-controlled islanded microgrid, IEEE Trans. Power Electron 30 (12) (2015) 7215–7229, https://doi.org/10.1109/TPEL.2015.2394351.

[20] H. Mahmood, D. Michaelson, J. Jiang, A power management strategy for PV/Battery hybrid systems in islanded microgrids, IEEE J Emerg Sel Top Power Electron 2 (4) (2014) 870–882, https://doi.org/10.1109/JESTPE.2014.2334051.

[21] D. Wu, F. Tang, T. Dragicevic, J.C. Vasquez, J.M. Guerrero, Autonomous active power control for islanded AC microgrids with photovoltaic generation and energy storage system, IEEE TransEnergy Conver 29 (4) (2014) 882–892, https://doi.org/10.1109/TEC.2014.2358612.

[22] Y. Shan, J. Hu, Z. Li, J.M. Guerrero, A model predictive control for renewable energy based AC microgrids without any PID regulators, IEEE Trans Power Electron 33 (11) (2018) 9122–9126, https://doi.org/10.1109/TPEL.2018.2822314.

[23] R. Heydari, Y. Khayat, M. Naderi, A. Anvari-Moghaddam, T. Dragicevic, F. Blaabjerg, A decentralized adaptive control method for frequency regulation and power sharing in autonomous microgrids, in: 2019 IEEE 28th International Symposium on Industrial Electronics (ISIE), IEEE, 2019, pp. 2427–2432.

[24] T.-.T. Nguyen, H.-.J. Yoo, H.-.M. Kim, Application of model predictive control to BESS for microgrid control, Energies 8 (8) (2015) 8798–8813.

[25] A.L. Bella, S.R. Cominesi, C. Sandroni, R. Scattolini, Hierarchical Predictive Control of Microgrids in Islanded Operation, IEEE Trans Automation Sci Eng 14 (2) (2017) 536–546, https://doi.org/10.1109/TASE.2016.2633397.

[26] C.A. Hans, P. Braun, J. Raisch, L. Grune, C. Reincke-Collon, Hierarchical Distributed Model Predictive Control of Interconnected Microgrids, IEEE Transactions on Sustainable Energy (2018) 1, https://doi.org/10.1109/TSTE.2018.2802922.

[27] Y. Li, Z. Zhang, S.A. Davari, C. Garcia, J. Rodriguez, FCS-MPC based primary control with improved performance for islanded AC Microgrids, in: 2020 11th Power Electronics, Drive Systems, and Technologies Conference (PEDSTC), IEEE, 2020, pp. 1–6.
[28] A. Bonfiglio, F. Delfino, M. Invernizzi, R. Procopio, P. Serra, An approximate methodology to verify the compliance of large photovoltaic power plants to system operator steady-state requirements, Electric Power Syst Res 127 (2015) 80–92, https://doi.org/10.1016/j.epsr.2015.05.015. Article volArt no. 4337.
[29] Z. Styczynski, P. Lombardi, R. Seethapathy, M. Piekutowski, C. Ohler, B. Roberts, Electric energy storage systems, in: CIGRE Working group C 6, 2011.
[30] F. Allgöwer, A. Zheng, Nonlinear Model Predictive Control, Birkhäuser, 2012.
[31] A. Bonfiglio, Modeling and Experimental Validation of an Islanded No-Inertia Microgrid Site, IEEE Trans Sustain Energy (2018) 1, https://doi.org/10.1109/TSTE.2018.2816401.
[32] A. Bonfiglio, M. Brignone, F. Delfino, M. Invernizzi, F. Pampararo, R. Procopio, A technique for the optimal control and operation of grid-connected photovoltaic production units, in: Proceedings of the Universities Power Engineering Conference, 2012, https://doi.org/10.1109/UPEC.2012.6398657 [Online]. Available, https://www.scopus.com/inward/record.uri?eid=2-s2.0-84872875108&partnerID=40&md5=0cd6d495431da0ec03ca59ce5e41d443.
[33] N. Mohan, T.M. Undeland, Power Electronics: Converters, Applications, and Design, John Wiley & Sons, 2007.
[34] A. Smets, K. Jäger, O. Isabella, M. Zeman, R. van Swaaij, Solar Energy, The physics and engineering of photovoltaic conversion. Technologies and Systems, UIT Cambridge, 2016.
[35] A. Bonfiglio, M. Brignone, M. Invernizzi, A. Labella, D. Mestriner, R. Procopio, A Simplified microgrid model for the validation of islanded control logics, Energies 10 (8) (2017) 1141 [Online]. Available, http://www.mdpi.com/1996-1073/10/8/1141.
[36] A. Labella, F. Filipovic, M. Petronijevic, A. Bonfiglio, R. Procopio, An MPC approach for grid-forming inverters: theory and experiment, Energies 13 (9) (2020) 2270 [Online]. Available, https://www.mdpi.com/1996-1073/13/9/2270.
[37] M. Fusero, A. Tuckey, A. Rosini, P. Serra, R. Procopio, and A. Bonfiglio, "A comprehensive inverter-BESS primary control for AC Microgrids," vol. 12, no. 20, p. 3810, 2019. [Online]. Available: https://www.mdpi.com/1996-1073/12/20/3810.
[38] ENTSO-E, Requirements for Grid connection applicable to all generators, in: European Network of Transmission System Operators for Electricity, ENTSO-E (2013 March), 2013.